J|A|C|S
ARTICLES
Published on Web 05/24/2006

Computational Simulations of HIV-1 Proteases—Multi-drug Resistance Due to Nonactive Site Mutation L90M

Hirotaka Ode,* Saburo Neya, Masayuki Hata, Wataru Sugiura,† and Tyuji Hoshino‡

Contribution from the Graduate School of Pharmaceutical Sciences, Chiba University, Chiba 263-8522, Japan

Received January 29, 2006; E-mail: odehir@graduate.chiba-u.jp

Abstract: Human immunodeficiency virus type 1 protease (HIV-1 PR) is one of the proteins that currently available anti-HIV-1 drugs target. Inhibitors of HIV-1 PR have become available, and they have lowered the rate of mortality from acquired immune deficiency syndrome (AIDS) in advanced countries. However, the rate of emergence of drug-resistant HIV-1 variants is quite high because of their short retroviral life cycle and their high mutation rate. Serious drug-resistant mutations against HIV-1 PR inhibitors (PIs) frequently appear at the active site of PR. Exceptionally, some other mutations such as L90M cause drug resistance, although these appear at nonactive sites. The mechanism of resistance due to nonactive site mutations is difficult to explain. In this study, we carried out computational simulations of L90M PR in complex with each of three kinds of inhibitors and one typical substrate, and we clarified the mechanism of resistance. The L90M mutation causes changes in interaction between the side chain atoms of the 90th residue and the main chain atoms of the 25th residue, and a slight dislocation of the 25th residue causes rotation of the side chain at the 84th residue. The rotation of the 84th residue leads to displacement of the inhibitor from the appropriate binding location, resulting in a collision with the flap or loop region. The difference in levels of resistance to the three inhibitors has been explained from energetic and structural viewpoints, which provides the suggestion for promising drugs keeping its efficacy even for the L90M mutant.

Introduction

Human immunodeficiency virus type 1 (HIV-1) proliferates under the assistance of its own aspartic protease, so-called HIV-1 protease (PR), in its life cycle.[1] HIV-1 PR is an enzyme composed of two identical polypeptides, each of which consists of 99 amino acid residues (Figure 1A), and has a function to process the viral Gag and Gag-Pol polyprotein precursors. Because this processing is essential for the viral maturation, the inhibition of PR function leads to an incomplete viral replication and prevents the infection of other cells.[2] Therefore, HIV-1 PR is an attractive target for anti-HIV-1 drugs. Seven PR inhibitors (PIs) have been approved by the FDA[3−9] and have successfully lowered the death rate due to acquired immune deficiency syndrome (AIDS) in advanced countries during the past decade. However, the emergence of PI-resistant mutants has become a serious problem in AIDS therapies.[10−13] The accumulation of multidrug-resistant mutations within HIV-1 PR makes it difficult to control viral replication in patients. Hence, PIs that maintain drug efficacy even for drug-resistant mutants are needed.

Most mutations causing a high level of drug resistance occur at the active site of HIV-1 PR. For example, D30N and G48V lead to specific resistance against nelfinavir (NFV) and saquinavir (SQV), respectively, and I84V shows multidrug resistance against several approved PIs.[7,10−18] Recent structural analyses by not only X-ray crystallography[19−28] but also computational

† AIDS Research Center, National Institute of Infectious Diseases, Musashimurayama, Tokyo 208-1011, Japan.
‡ Also PRESTO, JST, 4-1-8 Honcho Kawaguchi, Saitama, Japan.

(1) Kräusslich, H. G.; Wimmer, E. *Auu. Rev. Biochem.* **1988**, *57*, 701.
(2) Kohl, N. E.; Emini, E. A.; Schleif, W. A.; Davis, L. J.; Heimbach, J. C.; Dixon, R. A.; Scolinick, E. M.; Sigal, I. S. *Proc. Natl. Acad. Sci. U.S.A.* **1988**, *85*, 4686.
(3) Craig, J. C.; Duncan, I. B.; Hockley, D.; Grief, C.; Roberts, N. A.; Mills, J. S. *Antiviral Res.* **1991**, *16*, 295.
(4) Vacca, J. P.; et al. *Proc. Natl. Acad. Sci. U.S.A.* **1994**, *91*, 4096.
(5) Kempf, D. J.; et al. *Proc. Natl. Acad. Sci. U.S.A.* **1995**, *92*, 2484.
(6) Livington, D. J.; Pazhanisamy, S.; Porter, D. J.; Partaledis, J. A.; Tung, R. D.; Painter, G. R. *J. Infect. Dis.* **1995**, *172*, 1238.
(7) Patick, A. K.; et al. *Antimicrob. Agents Chemother.* **1996**, *40*, 292 (Erratum, *40*, 1575).
(8) Carrillo, A.; Stewart, K. D.; Sham, H. L.; Norbeck, D. W.; Kohlbrenner, W. E.; Leonard, J. M.; Kempf, D. J.; Molla, A. J. *J. Virol.* **1998**, *72*, 7532.
(9) Robinson, B. S.; et al. *Antimicrob. Agents Chemother.* **2000**, *44*, 2093.
(10) Condra, J. H.; et al. *Nature (London)* **1995**, *374*, 579.
(11) Kantor, R.; Fessel, W. J.; Zolopa, A. R.; Israelski, D.; Shulman, N.; Montoya, J. G.; Harbour, M.; Schapiro, J. M.; Shafer, R. W. *Antimicrob. Agents Chemother.* **2002**, *46*, 1086.
(12) Wu, T. D.; Schiffer, C. A.; Gonzales, M. J.; Taylor, J.; Kantor, R.; Chou, S.; Israelski, D.; Zolopa, A. R.; Fessel, W. J.; Shafer, R. W. *J. Virol.* **2003**, *77*, 4836.
(13) Johnson, V. A.; Brun-Vézinet, F.; Clotet, B.; Conway, B.; Kuritzkes, D. R.; Pillay, D.; Schapiro, J.; Telenti, A.; Richman, D. *Top. HIV Med.* **2005**, *13*, 125.
(14) Patick, A. K.; Duran, M.; Cao, Y.; Shugarts, D.; Keller, M. R.; Mazabel, E.; Knowles, M.; Chapman, S.; Kuritzkes, D. R.; Markowitz, M. *Antimicrob. Agents Chemother.* **1998**, *42*, 2637.
(15) Jacobsen, H.; Yasargil, K.; Winslow, D. L.; Craig, J. C.; Krohn, A.; Duncan, I. B.; Mous, J. *Virology* **1995**, *206*, 527.
(16) Jacobsen, H.; Hänggi, M.; Ott, M.; Duncan, I. B.; Andreoni, M.; Vella, S.; Mous, J. *Antiviral Res.* **1996**, *29*, 95.
(17) Jaconsen, H,; Hänggi, M.; Ott, M.; Duncan, I. B.; Owen, S.; Andreoni, M.; Vella, S.; Mous, J. *J. Infect. Dis.* **1996**, *173*, 1379.
(18) Ermolieff, J.; Lin, X.; Tang. J. *Biochemistry* **1997**, *36*, 12364.
(19) Mahalingam, B.; Louis, J. M.; Reed, C. C.; Adomat, J. M.; Krouse, J.; Wang, Y.-F.; Harrison, R. W.; Weber, I. T. *Eur. J. Biochem.* **1999**, *263*, 238.
(20) Hong, L.; Zhang, X. C.; Hartsuck, J. A.; Tang, J. *Protein Sci.* **2000**, *9*, 1898.

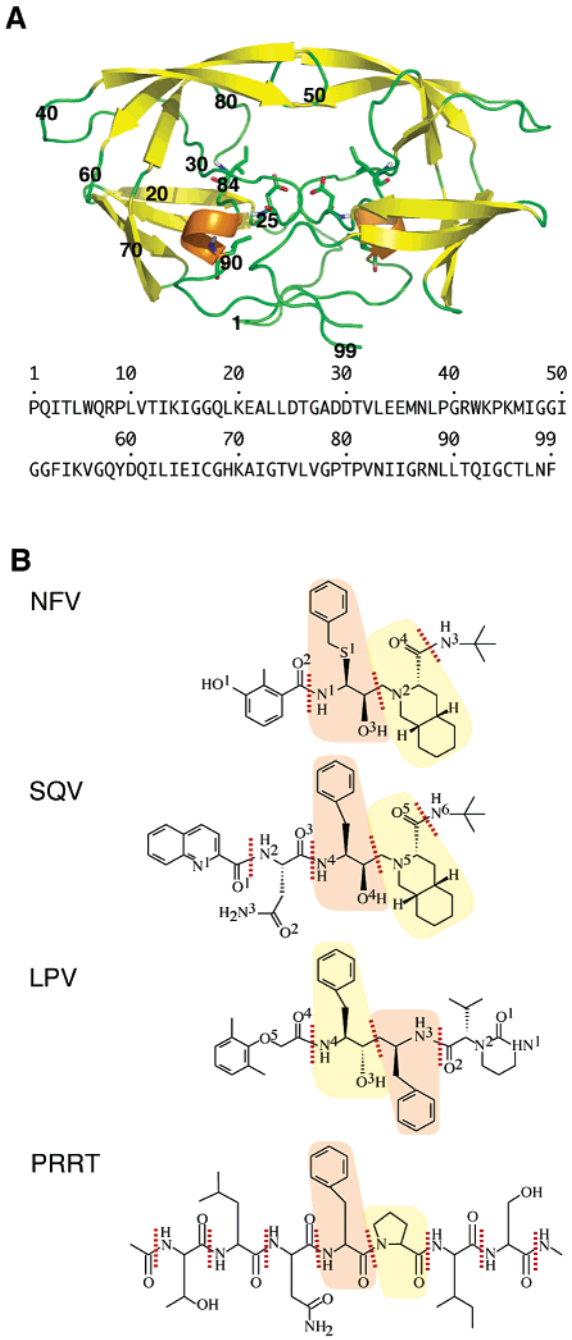

Figure 1. A: Structure of HIV-1 PR. Locations of the two catalytic aspartates, the 84th and the 90th residues, are shown in stick representation. The WT sequence of HIV-1 PR is shown below. B: Chemical structures of NFV, SQV, LPV, and PRRT. Each red dotted line shows a junction between subsites. The P1 subsite is highlighted with an orange background, and the P1′ subsite is highlighted with a yellow background.

studies[29−34] have revealed that these active site mutations changed direct interactions between PR and PI and caused unfavorable contact between them. Nonactive site mutations such as L10F and L90M have also been reported to cause a high level of resistance, although these residues cannot directly interact with PIs.[7,10−18] It is difficult to understand how nonactive site mutations lead to resistance against PIs. L90M is a primary mutation responsible for resistance against NFV and SQV.[7,14−17] L90M also appears to be associated with resistance to other PIs.[11−13] The structures of L90M PR mutants in complex with PIs have been determined through X-ray crystallographic approaches by some groups[20,26] and through our previous computational simulations.[33] These structures showed that the side chains of the mutated M90/M90′ altered their interactions with the catalytic aspartates D25/D25′. Additionally, L90M mutation affected local conformations at the 80's loop of PR, which is quite far from the location of the 90th residues. The mechanism of resistance due to L90M, however, is still not clear, and a strategy for the design of potent drugs against L90M-acquired virus has not yet been established.

In this study, we carried out computational simulations of L90M PR in complex with several kinds of ligands to clarify the mechanism of resistance due to L90M. NFV, SQV, and lopinavir (LPV) were selected as representative PI inhibitors currently used in the clinical field (Figure 1B). NFV and SQV lose their ability to inhibit PRs that have acquired L90M mutation. In contrast, single mutations have little effect on the inhibition ability of LPV.[35] In addition, the oligopeptide at the PR/RT cleavage site (PRRT) was selected as a typical substrate for the enzyme to investigate the effect of L90M on substrate binding (Figure 1B). The PR/RT cleavage site contains Phe-Pro at the P1−P1′ residues (notation by Schecter and Berger[36]). It is unusual for mammalian endopeptidases to cleave the peptide bond located at the N-terminal side of Pro, and this cleavage site is specific to HIV-1 PR.[37,38] This cleavage mechanism is unique as reported previously.[39−41] Therefore, the structure of PRRT was used as the base of drug design for NFV, SQV, and some PIs.[3,7,42] In this study, the binding energies of NFV, SQV, LPV, and PR/RT were first calculated to compare the levels of resistance of the wild type (WT) and L90M mutant. The binding structures were then compared in two groups of inhibitors: one groups consisting of HIV inhibitors that lose drug efficacy due

(21) Mahalingam, B.; Louis, J. M.; Hung, J.; Harrison, R. W.; Weber, I. T. *Proteins* **2001**, *43*, 455.
(22) Mahalingam, B.; Boross, P.; Wang, Y.-F.; Louis, J. M.; Fischer, C. C.; Tozser, J.; Harrison, R. W.; Weber, I. T. *Proteins* **2002**, *48*, 107.
(23) Weber, J.; et al. *J. Mol. Biol.* **2002**, *324*, 739.
(24) King, N. M.; Melnick, L.; Prabu-Jeyabalan, M.; Nalivaika, E. A.; Yang, S. S.; Gao, Y.; Nie, X.; Zepp, C.; Heefner, D. L.; Schiffer, C. A. *Protein Sci.* **2002**, *11*, 418.
(25) Prabu-Jeyabalan, M.; Nalivaika, E. A.; King, N. M.; Schiffer, C. A. *J. Virol.* **2003**, *77*, 1306.
(26) Mahalingam, B.; Wang, Y.-F.; Boross, P. L.; Tozser, J.; Louis, J. M.; Harrison, R. W.; Weber, I. T. *Eur. J. Biochem.* **2004**, *271*, 1516.
(27) King, N. M.; Prabu-Jeyabalan, M.; Nalivaika, E. A.; Wigerinck, P.; Béthune, M. P.; Schiffer, C. A. *J. Virol.* **2004**, *78*, 12012.
(28) Prabu-Jeyabalan, M.; Nalivaika, E. A.; King, N. M.; Schiffer, C. A. *J. Virol.* **2004**, *78*, 12446.
(29) Rick, S. W.; Topol, I. A.; Erickson, J. W.; Burt, S. K. *Protein Sci.* **1998**, *8*, 1750.
(30) Piana, S.; Carloni, P.; Rothlisberger, U. *Protein Sci.* **2002**, *11*, 2393.
(31) Clemente, J. C.; Hermrajani, R.; Blum, L. E.; Goodenow, M. M.; Dunn, B. M. *Biochemistry* **2003**, *42*, 15029.
(32) Perryman, A. L.; Lin, J.-H.; McCammon, J. A. *Protein Sci.* **2003**, *13*, 1108.
(33) Ode, H.; Ota, M.; Neya, S.; Hata, M.; Sugiura, W.; Hoshino, T. *J. Phys. Chem. B* **2005**, *109*, 565.
(34) Wittayanarakul, K.; Aruksakunwong, O.; Saen-oon, S.; Chantratita, W.; Parasuk, V.; Sompornpisut, P.; Hannongbua, S. *Biophys. J.* **2005**, *88*, 867.
(35) Kempf, D. J.; Isaacson, J. D.; King, M. S.; Brun, S. C.; Xu, Y.; Real, K.; Bernstein, B. M.; Japour, A. J.; Sun, E.; Rode, R. A. *J. Virol.* **2001**, *75*, 7462.
(36) Schechter, I.; Berger, A. *Biochem. Biophys. Res. Commun.* **1967**, *27*, 157.
(37) Pearl, L. H.; Taylor, W. R. *Nature (London)* **1987**, *328*, 482.
(38) Darke, P. L.; Nutt, R. F.; Brady, S. F.; Garsky, V. M.; Ciccarone, T. M.; Leu, C.-H.; Lumma, P. K.; Freidinger, R. M.; Veber, D. F.; Sigal, I. S. *Biochem. Biophys. Res. Commun.* **1988**, *156*, 297.
(39) Okimoto, N.; Tsukui, T.; Hata, M.; Hoshino, T.; Tsuda, M. *J. Am. Chem. Soc.* **1999**, *121*, 7349.
(40) Okimoto, N.; Tsukui, T.; Kitayama, K.; Hata, M.; Hoshino, T.; Tsuda, M. *J. Am. Chem. Soc.* **2000**, *122*, 5613.
(41) Okimoto, N.; Kitayama, K.; Hata, M.; Hoshino, T.; Tsuda, M. *J. Mol. Struct. (THEOCHEM)* **2001**, *543*, 53.
(42) Roberts, N. A.; et al. *Science* **1990**, *248*, 358.

to L90M mutations, such as NFV and SQV, and the other group consisting of drugs that maintain efficacy, such as LPV. Prominent differences between the two groups were seen at the contact of M90 to D25, shifts of D25, rotation of the side chains of I84, displacement of the flap region of I50, and deformation of the loop region of P81. D25, I84, I50, and P81 are all located at the active site of the PR. Detail discussion are developed in contrast with the resistivity of PR. Our findings provide information for designing better inhibitors that maintain drug efficacy despite L90M or other nonactive site mutations.

Materials and Methods

Molecular Dynamics Simulation. Before carrying out molecular dynamics (MD) simulations, quantum chemical calculations were executed for PIs to deduce the atom charges utilized in MD simulations. Geometry optimization was performed on each PI, and the electrostatic potential was calculated at the B3LYP/6-31G(d,p) level using the Gaussian03 program.[43] The partial atom charges were determined using the RESP method[44] so that the atom charges could reproduce the values of the calculated electrostatic potential at the surrounding points of the PI. Charges were set equal between two atoms if they were the same element and had the same bond coordination. Minimizations and MD simulations were carried out using the Sander module of the AMBER7 package.[45] The AMBER ff02 force field[46] was used as the parameters for van der Waals and bonded energy terms basically, and the general AMBER force field[47] was used as the parameters for NFV, SQV, and LPV.

Each initial structure for the clade B HXB2 PRs in complex with NFV, SQV, and LPV was modeled from the atom coordinates of the X-ray crystal structure (PDB code: 1OHR,[48] 1HXB,[42,49] and 1MUI,[50] respectively) using the LEaP module (Figure 1A). The initial structure for the PR in complex with PRRT before the catalytic reaction was modeled in the same manner as that previously reported.[39] The oligopeptide of ACE-THR-LEU-ASN-PHE-PRO-ILE-SER-NME was utilized as PRRT, and one water molecule was inserted between PRRT and D25/D25′. Each model was placed in a rectangular box filled with about 8000 TIP3P water molecules,[51] with all of the crystal water molecules remaining. One water molecule was added between LPV and I50/I50′ in the LPV complex model, because no crystal water molecule was present in the crystallographic data. It is known that the hydrogen bonds between PI and I50/I50′ via the water molecule are critically important for PI binding with HIV-1 PR.[33,39−41] The cutoff distance for the long-range electrostatic and the van der Waals energy terms was set at 12.0 Å. All covalent bonds to hydrogen atoms were constrained using the SHAKE algorithm.[52] Periodic boundary conditions were applied to avoid edge effects in all calculations. Energy minimization was achieved in three steps. At first, movement was allowed only for the water molecules and ions. Next, the ligand and the mutated residues were allowed to move in addition to the water molecules and ions. Finally, all atoms were permitted to move freely. In each step, energy minimization was executed by the steepest descent method for the first 1000 steps and the conjugated gradient method for the subsequent 3000 steps. After 52.0 ps heating calculation until 300 K using the NVT ensemble, 1.5 ns equilibrating calculation was executed at 1 atm and at 300 K using the NPT ensemble, with an integration time step of 1.0 fs. In the present calculations, the MD simulations showed no large fluctuations after about 500 ps equilibrating calculation (Supporting Information Fig. S1). Hence, atom coordinates were collected at the interval of 0.5 ps for the last 500 ps to analyze the structure in detail.

Protonation States. The protonation states of catalytic aspartates D25 and D25′ vary depending on the binding inhibitors or substrates. Hence, the appropriate protonation states of catalytic aspartates should be determined for the respective ligands. For NFV, the protonated state was already determined in our previous study.[33] That is, D25 was protonated and D25′ was unprotonated in each of WT PR and L90M PR in complex with NFV. To determine the protonation states when SQV or LPV binds to the WT PR, the total energies of the two kinds of complexes were compared after energy minimization. One complex represented a combination of protonated D25/unprotonated D25′ states, and the other represented the opposite combination. This comparison clearly suggested the preference of the protonated D25 and unprotonated D25′ states (Supporting Information Table S1 A). In contrast to the case of WT PR, we used another method to determine the protonation states of L90M PR with SQV or LPV because they might have greatly different conformation from the respective crystal structures. Hence, we executed 1.5 ns MD simulations of the two protonation states in these models and compared the total energies of the two protonation states for the last 500 ps of the simulations. The energy comparison indicated that L90M PR in complex with each of SQV and LPV preferred the protonated D25 and unprotonated D25′ states (Supporting Information Table S1 B). For both WT and L90M PR with PRRT, the D25 unprotonated and D25′ protonated states were selected so that the hydrolysis reaction could proceed as described in a previous paper.[39]

Binding Energy Calculation (MM/PBSA). The binding free energy[53] was calculated by the following equation:

$$\Delta G_{\mathrm{b}} = \Delta G_{\mathrm{MM}} + \Delta G_{\mathrm{sol}} - T\Delta S$$

where ΔG_{b} is the binding free energy in solution, ΔG_{MM} is the molecular mechanics (MM) interaction energy, ΔG_{sol} is the solvation energy, and $-T\Delta S$ is the contribution of conformational entropy to the binding. Since the contribution of conformational entropy to the change of ΔG_{b} is negligible among the mutants as pointed out by Massova,[54] the last entropy term in the energy estimation was neglected. ΔG_{MM} was calculated by the following equation:

$$\Delta G_{\mathrm{MM}} = \Delta G_{\mathrm{int}}^{\mathrm{ele}} + \Delta G_{\mathrm{int}}^{\mathrm{vdw}>}$$

where $\Delta G_{\mathrm{int}}^{\mathrm{ele}}$ and $\Delta G_{\mathrm{int}}^{\mathrm{vdw}}$ are electrostatic and van der Waals interaction energies between a ligand and a protein. These energies were computed using the same parameter set as that used in the MD simulation, and no cutoff was applied for the calculation. Solvation energy ΔG_{sol} can be divided into two parts:

$$\Delta G_{\mathrm{sol}} = \Delta G_{\mathrm{sol}}^{\mathrm{ele}} + \Delta G_{\mathrm{sol}}^{\mathrm{nonpol}}$$

The electrostatic contribution to the solvation free energy ($\Delta G_{\mathrm{sol}}^{\mathrm{ele}}$) was calculated by the Poisson−Boltzmann (PB) method using the DelPhi program.[55] The hydrophobic contribution to the solvation free energy ($\Delta G_{\mathrm{sol}}^{\mathrm{nonpol}}$) was determined with a function of the solvent-accessible surface-area.[56]

Hydrogen Bond Criterion. The formation of a hydrogen bond was defined in terms of distance and orientation. The combination of donor

(43) Frisch, M. J.; et al. *Gaussian 03*; Gaussian, Inc., Wallingford CT, 2004.
(44) Cieplak, P.; Cornell, W. D.; Bayly, C.; Kollman, P. A. *J. Comput. Chem.* **1995**, *16*, 1357.
(45) Case, D. A.; et al. *AMBER 7*; University of California: San Francisco, 2002.
(46) Wang, J.; Cieplak, P.; Kollman, P. A. *J. Comput. Chem.* **2000**, *21*, 1049.
(47) Wang, J.; Wolf, R. M.; Caldwell, J. W.; Kollman, P. A.; Case, D. A. *J. Comput. Chem.* **2004**, *25*, 1157.
(48) Kaldor, S. W.; et al. *J. Med. Chem.* **1997**, *40*, 3979.
(49) Krohn, A.; Redshaw, S.; Ritchie, J. C.; Graves, B. J.; Hatada, M. H. *J. Med. Chem.* **1991**, *34*, 3340.
(50) Stoll, V.; et al. *Bioorg. Med. Chem.* **2002**, *10*, 28032.
(51) Jorgensen, W. L.; Chandrasekhar, J.; Madura, J. D.; Impey, R. W.; Klein, M. L. *J. Chem. Phys.* **1983**, *79*, 926.
(52) Ryckaert, J.-P.; Ciccotti, G.; Berendsen, H. J. C. *J. Comput. Phys.* **1977**, *23*, 327.
(53) Kollman, P. *Chem. Rev.* **1993**, *93*, 2395.
(54) Massova, I.; Kollman, P. A. *Perspect. Drug. Discovery Des.* **2000**, *18*, 113.
(55) Honig, B.; Nicholls, A. *Science* **1995**, *268*, 1144.
(56) Sitkoff, D.; Sharp, K. A.; Honig, B. *J. Phys. Chem.* **1994**, *98*, 1978.

Table 1. Binding Energies of Each Model[a]

		ΔG_{int}^{ele}	ΔG_{int}^{vdw}	ΔG_{sol}	ΔG_b[b]	ΔG_b[c]	resistant level[d]
NFV	WT	−24.4 ± 3.6	−66.6 ± 3.6	37.5 ± 3.3	−53.5 ± 4.2	+2.8	5
	L90M	−20.2 ± 3.8	−64.1 ± 3.1	33.6 ± 3.5	−50.7 ± 4.6		
SQV	WT	−29.6 ± 4.7	−71.5 ± 4.0	34.7 ± 3.6	−66.4 ± 5.2	+2.7	3.5
	L90M	−27.9 ± 4.2	−72.9 ± 3.8	37.1 ± 3.6	−63.7 ± 4.7		
LPV	WT	−31.2 ± 4.8	−71.1 ± 3.7	41.0 ± 3.4	−61.8 ± 4.5	−0.3	∼1
	L90M	−29.8 ± 5.2	−74.1 ± 3.2	41.9 ± 3.4	−62.1 ± 4.9		
PRRT	WT	−74.7 ± 9.3	−84.1 ± 4.2	91.7 ± 5.3	−67.2 ± 7.5	−0.5	-
	L90M	−72.4 ± 6.3	−84.7 ± 4.7	89.4 ± 4.7	−67.7 ± 5.4		

[a] Energy is presented in units of kcal/mol. [b] $T\Delta S$ is not included. [c] $\Delta\Delta G_b = \Delta G_b(\text{L90M}) - \Delta G_b(\text{WT})$ [d] Resistance level was taken from refs 7, 18, and 35. Resistance level is defined as IC90(L90M)/IC90(WT) or as IC50(L90M)/IC50(WT) in the references.

D, hydrogen H, and acceptor A atoms with a D−H···A configuration was regarded as a hydrogen bond when the distance between donor D and acceptor A was shorter than R_{max}(= 3.5 Å) and the angle H−D−A was smaller than Θ_{max}(= 60.0°).

Results

Binding Energy Calculations. The influence of L90M mutation on binding energy ΔGb was examined for each ligand. Table 1 shows the results of MM/PBSA calculations for the WT and L90M PR in complex with each ligand. L90M reduced the binding energies of NFV and SQV. Results of some experiments have suggested that L90M mutation caused resistance against these inhibitors.[7,11−18] On the other hand, L90M PR exhibits almost the same affinity as that of WT PR for LPV. It has been reported that the affinity of LPV was hardly affected by any single mutations.[35] Hence, the results of our simulations are compatible with the results of previous experimental analyses. The affinity of L90 M PR with PRRT is almost the same as that of WT PR.

Hydrogen Bonds between PR and Ligands. Hydrogen bonds play an essential role in stabilizing protein−ligand complexes. We examined 1000 snapshots during the last 500 ps and identified direct or one water molecule-mediated hydrogen bonds (Supporting Information Table S2). NFV mainly creates hydrogen bonds with D25′ and D30 in the WT model. In contrast, NFV interacts with D25 and D25′ in L90M PR. That is, NFV hardly interacts with D30 in the L90M model. It is known that D30 contributes significantly to PR−NFV binding and that the mutation D30N causes specific resistance against NFV.[7,14,57,58] Moreover, in WT and L90M PR, one water molecule is located between I50/I50′ and NFV. This water molecule creates hydrogen bonds with I50′ of WT PR (99.8% of the bonds being maintained during the last 500 ps of simulation) and with I50 of L90M PR (92.4%), while these hydrogen bonds are often broken with NFV in each model (∼50%). SQV has a direct interaction with D25′ and a one water molecule-mediated interaction with I50′ in both WT and L90M models. In addition, the main chain at the P2 subsite of SQV makes a hydrogen bond with G48 in both models. In contrast, the side chain at the P2 subsite (−$CONH_2$) interacts with different residues in the two models. The side chain interacts with G48 in the WT model and with D30 in the L90M model. Interestingly, G48 is a residue whose mutation causes specific resistance against SQV.[15−18] Thus, both NFV and SQV lose significant hydrogen bonds due to L90M mutation. On the other hand, LPV has similar hydrogen bond networks in the WT and L90M models. LPV creates direct hydrogen bonds with D25, D25′, and D29. One water molecule connects LPV to the 50th residues by hydrogen bonding. PRRT has similar interactions with D29, D30, and G48 in S4−S1 pockets in the WT and L90M models. However, PRRT has different interactions in S1′-S4′ pockets. One water molecule also stays between D25/D25′ and PRRT in the PR model, while it hardly makes any stable hydrogen bond.

Comparison of the Structures of the WT and L90M Models. To clarify the effect of mutation at the 90th residue on active site conformation, the average structure of the L90M model for the last 500 ps was compared with that of the corresponding WT model. The L90M model was fitted to the WT model using the coordinates of the main chain atoms N, Cα, and C, and the root-mean-squared deviation (RMSD) value was calculated (Figure 2). When the structures of each ligand in the WT and L90M models were compared, some atoms of NFV and SQV were found to exhibit large RMSD values (>2.0 Å). Atoms at the thio-phenol group (−$S-C_6H_5$) in NFV are dislocated to a quite different position, and all of the atoms in SQV are shifted in the same direction. On the other hand, no atoms in LPV exhibit such large RMSD values. In the case of PRRT, the P4−P1′ subsites have almost identical conformations, but there is a prominent difference at the P2′-P4′ subsite. The tertiary structures of the WT PR and L90M PR were also compared. RMSD 3D plots clearly indicate that deviation in the NFV complex model is markedly large compared to other ligand-bound cases. In the case of NFV, main chain atoms at the flap and at P79′ and its neighboring residues show large differences in WT PR and L90M PR. We previously reported conformational changes at the same residues.[33] There are small differences between the results of the present study and those of the previous study regarding the residues at the flap region. Namely, the flap region shows larger deviation from the WT in the present calculation. This is because the residues are flexible (Supporting Information Figure S2) and we examined larger sets of coordinates in this study (1000 sets of coordinates from 1 to 1.5 ns) than the previous study (200 sets of coordinates from 0.9 to 1.0 ns). L90M PR in complex with SQV shows local conformational changes at P81 and its neighbors. In the case of LPV, the main chain atoms at the active site are hardly affected by L90M mutation, although some atoms at the nonactive site show large deviations. In the case of PRRT, the main chain atoms at I50′ and its neighbors show noticeable deviations.

Mechanism of Conformational Changes at the Active Site. Figure 2 shows that L90M mutation affects the location of the

(57) Sugiura, W.; et al. *Antimicrob. Agents Chemother.* **2002**, *46*, 708.
(58) Sugiura, W.; et al. *Jpn. J. Infect. Dis.* **1999**, *52*, 175.

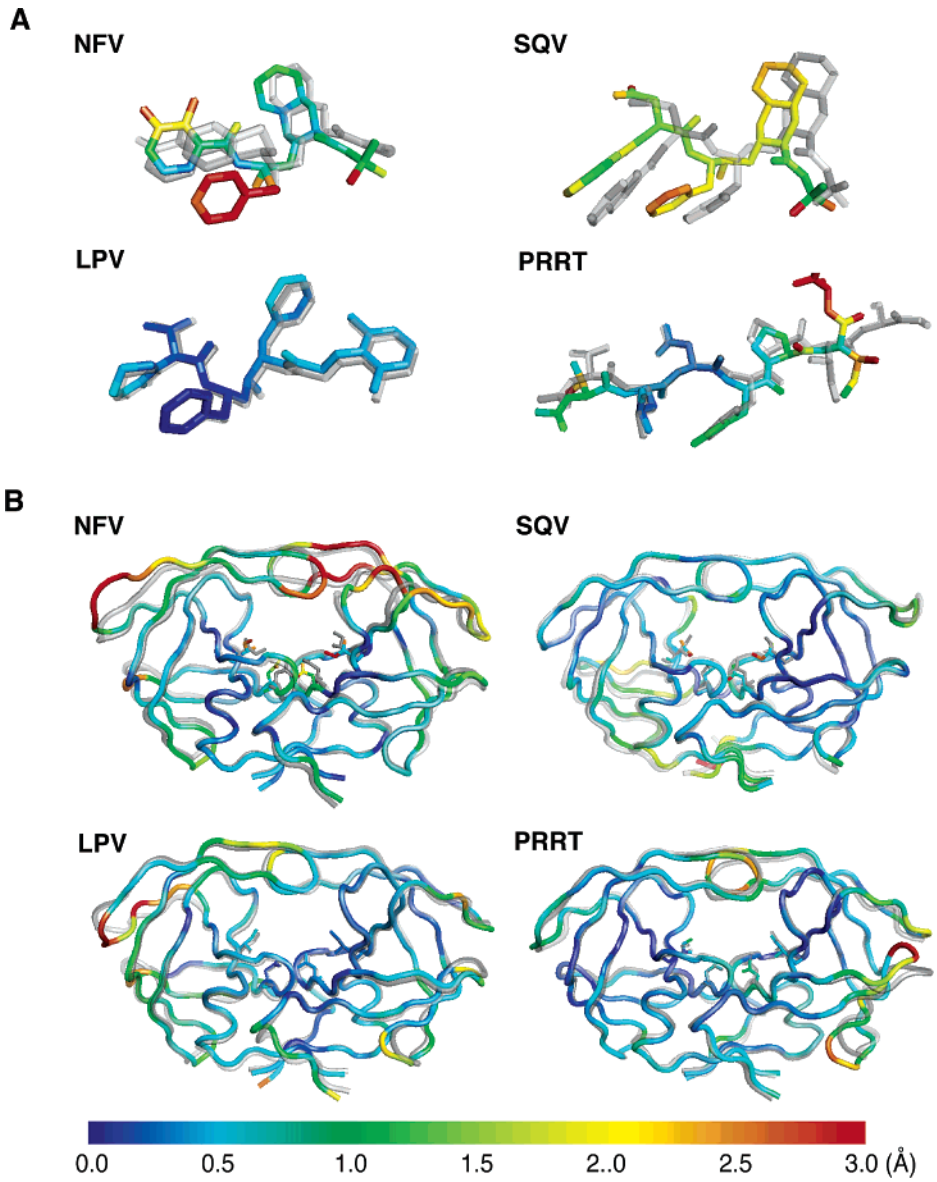

Figure 2. 3D plots of RMSD between the average structures of WT and L90M models. **A**: Ligands in the L90M model are shown as colored sticks. **B**: PRs in the L90M model are shown in colored tube representation, and D25/D25′ and I84/I84′ are shown in stick representation. The color means the magnitude of RMSD shown in the bottom bar. The L90M model was fitted on the WT model using the coordinates of main chain atoms N, Cα, and C of PR. The superimposed gray sticks and tubes represent the structure of the WT model.

ligand and the tertiary conformation of the active site of PR. To determine the reason for induction of these conformational changes at the active site by the nonactive site mutation L90M, conformations of the catalytic triad D25T26G27/D25′T26′G27′ have been examined in detail. These residues have van der Waals contacts with the side chains of the 90th residues[20,26,33] and are located at the active site. In NFV, SQV, and PRRT complex models, some residues showed about 1.0 Å deviations between WT and L90M PR (Supporting Information Table S3). On the other hand, the deviations of all of these residues in the LPV complex model are about 0.5 Å. These residues are the least fluctuating residues in PR because they create rigid hydrogen bond networks, so-called fireman grips[59] (Supporting Information Fig. S2). The root-mean-squared fluctuations (RMSF) of these residues were about 0.3 Å. Thus, these conformational changes at these triads are critically important. In the case of NFV, SQV, and PRRT complex models, D25 Cβ -D25′ Cβ distances are also different between the WT and

Table 2. Distances between D25 Cβ-D25′ Cβ, D25 Cβ-I84 Cβ, and 25′ Cβ-I84′ Cβ[a]

D25Cβ-D25′Cβ	NFV	SQV	LPV	PRRT
WT	6.2 ± 0.1	6.7 ± 0.2	7.1 ± 0.2	7.3 ± 0.3
L90M	6.5 ± 0.2	6.2 ± 0.1	7.0 ± 0.2	7.6 ± 0.2
Δ[b]	0.3	−0.5	0.1	0.3
D25Cβ-I84Cβ	NFV	SQV	LPV	PRRT
WT	5.6 ± 0.2	5.0 ± 0.2	4.7 ± 0.2	4.4 ± 0.3
L90M	5.0 ± 0.3	5.1 ± 0.2	4.9 ± 0.2	4.4 ± 0.3
Δ[b]	−0.6	0.1	0.2	0.0
D25′Cβ-I84′Cβ	NFV	SQV	LPV	PRRT
WT	4.4 ± 0.2	5.4 ± 0.4	5.2 ± 0.2	5.0 ± 0.2
L90M	5.8 ± 0.3	5.8 ± 0.2	5.2 ± 0.2	5.1 ± 0.2
Δ[b]	1.4	0.4	0.0	0.1

[a] Distances are presented in units of Å. [b] Difference between L90 M and WT.

(59) Strisovsky, K.; Tessmer, U.; Langner, J.; Konvalinka, J.; Kräusslich, H.-G. *Protein Sci.* **2000**, *9*, 1631.

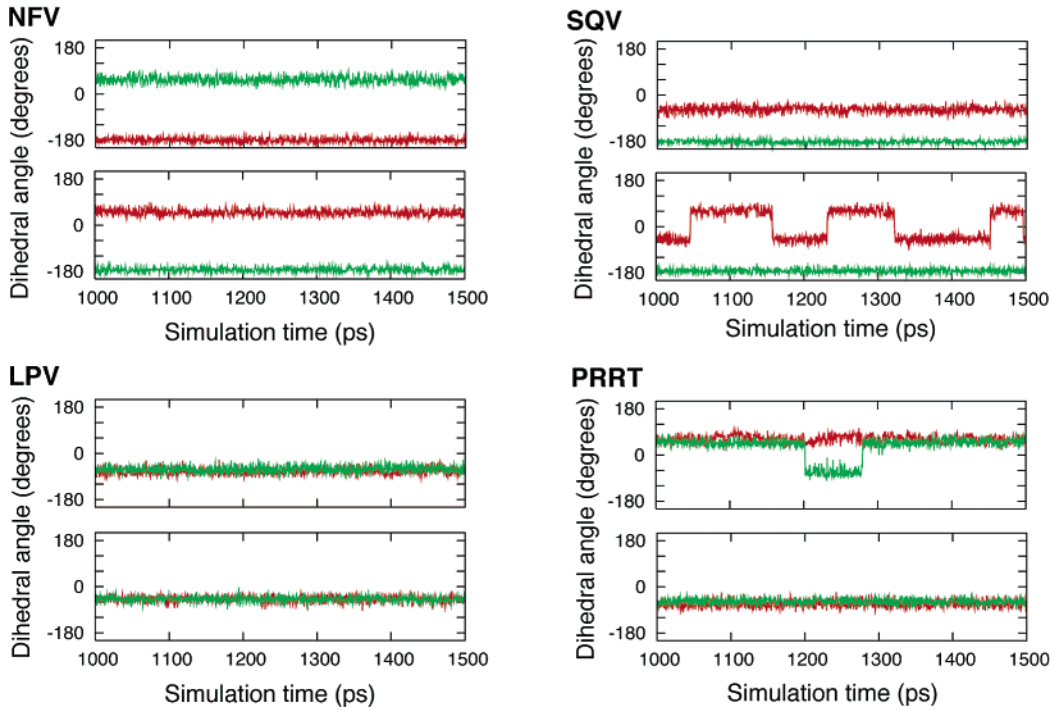

Figure 3. Dihedral angles of N−Cα−Cβ−Cγ1 of I84 (upper) and I84′ (lower) during the last 500 ps of simulations. Red lines represent the WT model, and green lines represent the L90M model.

L90M models (Table 2). There is a particularly large difference in orientations of the side chains of D25/D25′. Furthermore, in the case of NFV and SQV, rotations occur at the side chains of I84/I84′, which are active site residues and are in contact with the side chains of D25/D25′ (Figure 3). The rotations are correlated with the changes in distances between D25 Cβ and I84 Cβ and between D25′ Cβ and I84′ Cβ. That is, the rotations are induced by displacements of the catalytic aspartates D25 and D25′. The side chains of I84/I84′ have large hydrophobic contacts with the ligands, and the structure of the active site is deformed asymmetrically. Consequently, we speculate that the following mechanism causes the active site conformational changes. First, L90M mutation changes the interaction between the 90th residues and D25/D25′. Second, D25/D25′ is shifted. Third, I84/I84′ show rotations of their side chains. Finally, the interaction between ligands and I84/I84′ causes conformational changes of the active site.

Discussion

In HIV-1 PR, the 90th residue is located at the dimer interface, that is, out of the substrate-binding pocket. Hence, it has no direct contact with any ligand of PR. Despite its location, L90M mutation causes resistance against FDA-approved PIs, such as NFV and SQV.[7,11−18] It is difficult to imagine the mechanism of resistance due to L90M mutation. Several X-ray crystal structures have ever been provided for L90M PR.[20−22,26] These structures showed that the side chains of the mutated M90/M90′ altered the interactions with the catalytic aspartates D25/D25′. Hong et al. determined the crystal structure of G48V/L90M HIV-1 PR in complex with SQV. They proposed that alteration in the interactions between the 90th residues and D25/D25′ led to reduction of structural flexibility at the main chains of the catalytic triads and lowered the possibility of these main chains making structural adjustments to SQV.[20] Mahalingam et al. determined the structure of L90M HIV-1 PR in complex with IDV and with substrate analogue inhibitors. They further analyzed kinetic characteristics of L90M mutants and reported that L90M appeared to indirectly lower the dimer stability.[21,22,26] Our recent study in which computational simulations of HIV-1 PR in complex with NFV were carried out suggested that L90M mutation caused a decrease of binding energies and that conformational changes appeared at the flap and 80's loop regions, which are distant from the 90th residues.[33] Hence, for NFV, we concluded that the drug resistance due to L90M was caused by these active site conformational changes. Despite the accumulation of these experimental and theoretical findings, there has been no clear suggestion for drug designs to reduce the degree of or prevent the drug resistance due to L90M.

In this study, investigations of L90M PR were carried out for the purpose of establishing a strategy for promising drug design, and the structures of L90M PR in complexes with NFV, SQV, LPV, and a substrate at the PR/RT cleavage site (PRRT) were analyzed in detail. NFV and SQV lose their inhibitory efficacy for L90M mutation.[7,14−18] In contrast, LPV hardly changes its affinity with PR despite the L90M mutation.[35] The substrate PRRT has a unique sequence, Phe-Pro, at P1/P1′ subunits, whose structure is the basis for the drug design for NFV, SQV, and other PIs.[3,42] In all computed models, changes in interaction between catalytic aspartates D25/D25′ and the 90th residues occur due to the L90M mutation. In contrast, different responses have been observed at the active site of PR in the models. In the L90M PR/NFV complex, L90M causes large conformational changes at the active site, especially at the flap and 80's loop regions of PR. The L90M mutation also causes dislocations of side chains of D25/D25′ and rotations of side chains of I84/I84′. In the L90M PR/SQV complex, a positional shift of SQV and local conformational change at 80's loop

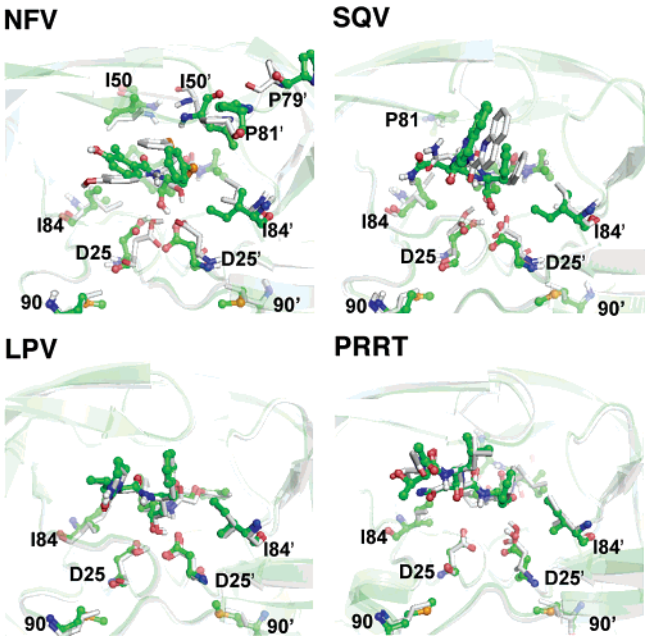

Figure 4. Structure around the active site. Each PR in the L90M model is shown in green cartoon, and each of the ligands and important residues is shown in green ball-and-stick representation. The superimposed gray cartoons and sticks represent the structure of the WT model.

regions occur. Dislocations of the side chains of D25/D25′ and rotations of I84/I84′ also occur, as in the L90M PR/NFV complex. These conformational changes have also been observed in the crystal structure of G48V/L90M PR/SQV complex (PDB code: 1FB7[20]) when compared with WT PR/SQV complex (PDB code: 1HXB[42,49]). In addition, a comparison of the structure of L90M PR in complex with SQV and the crystal structure of G48V/L90M PR/SQV complex shows that the 80's loop, where L90M causes conformational changes, is located at similar positions in the two structures (Supporting Information Figure S3). In the complex with each of these two inhibitors, L90M mutation induces common effects: dislocations of the 25th residues and rotations of the side chains of the 84th residues. In addition, L90M PR decreases the binding energy with each of NFV and SQV, which would reflect the positional shift of the inhibitors. In contrast, in the L90M PR/LPV complex, conformational changes hardly occur at the active site. Dislocations of the 25th residues and rotations of the side chains of the 84th residues hardly appear. Energetically, LPV exhibits the same binding affinity with L90M and WT PRs. PRRT also exhibits the same affinity with L90M and WT PRs, although conformations at both of the residues near I50/I50′ and P2′-P4′ subunits of PRRT are greatly changed. In the PRRT model, no rotation of the side chains of 84I/84′I occurs, while the distance between the two side chains of D25 and D25′ is changed. These results indicate that rotations of the side chains of I84/I84′ are involved in the resistance due to L90M. Consequently, we can conclude that the mechanism of resistance due to L90M is rotations of the side chains of the 84th residues due to dislocations of the side chains of the 25th residues, which are initiated by changes in the interactions between the 90th and the 25th residues. These rotations change the shapes of the active sites, and the change decreases the interactions between PR and ligands (Figure 4). There is still the question of why rotation of the 84th side chains occurs when L90M PR is bound with NFV or SQV but does not occur when L90M PR is bound with LPV and PRRT. The answer to this question is that the rotations is due to not only to dislocations of side chains of D25/D25′ but also to the geometry of the ligand. The shift in side chains of 25D/25′D occurs when L90M PR is bound with NFV, SQV, and PRRT. Focusing on the P1/P1′ subsites of those ligands, NFV and SQV each contain a dodecahydroisoquinoline ring, which is a rigid and bulky functional group, and PRRT has a ring of PRO. These rings are located near D25/D25′ and assist the dislocation of the side chains of D25/D25′ because of their rigidity. Moreover, the size of the rings is responsible for the rotation of the side chains of I84/I84′. Rotation of the side chains of the 84th residues occurs when L90M PR is bound with NFV or SQV. In contrast, rotation hardly occurs despite the side chain dislocations of D25/D25′ when L90M PR is bound with PRRT. The ring size of PRRT is smaller than those of NFV and SQV and makes no unfavorable collision with side chains of I84/I84′. Consequently, the size and flexibility of P1/P1′ subsites of the ligand are closely related to the resistance due to L90 M. We speculate that a single L90M mutation has little effect on the binding affinity with a ligand that has a linear group or a small ring at its P1/P1′ subsite.

We further investigated the interactions between the ligands and each amino acid residue of PRs by performing fragment molecular orbital (FMO) calculations.[60] In the FMO scheme, the total system is divided into fragments and calculations are carried out in parallel, which makes it possible to adopt the ab initio MO calculation for a large molecule like a protein. The single point energy of each model was calculated at the FMO−HF/6-31G level using the ABINIT-MP program[61] The model structures were constructed by the following two steps. First, the average structure was calculated on the basis of 1000 coordinates acquired during the last 500 ps of MD simulation. Next, energy minimization was executed on the average structure. One amino acid residue or one inhibitor was set as a single fragment. It was confirmed from the computational results shown in Figure 5 that each of the ligands indeed interacts with the active site residues or their neighboring residues. Notably, LPV and PRRT interact with only several active site residues. That is, the residues they interact with are quite limited compared with those with which NFV and SQV interact. Furthermore, LPV shows no significant difference between its interactions in WT and L90M PRs. LPV has highly specific interactions with D29 and D25′, whose mutations inactivate the function of the PR.[2,62] Figure 5 also indicates that NFV and SQV show noticeable loss of interaction energies with several residues in both the WT and L90M models. In particular, NFV has unfavorable contact with K45, R87, R8′, D29′, and D30′, and SQV has unfavorable contact with D25′ and D29′. In contrast, LPV shows little energetical loss in the interaction with protein residues in both models. Accordingly, we speculate that this specificity and the little energetical loss are also reasons why L90M mutation has little effect on the binding of LPV.

Last, we investigated whether simulations can provide the correct order in terms of potency of the inhibitors. In the

(60) Kitaura, K.; Sawai, T.; Asada, T.; Nakano, T.; Uebayasi, M. *Chem. Phys. Lett.* **1999**, *312*, 319.
(61) Nakano, T.; Kaminuma, T.; Sato, T.; Fukuzawa, K.; Akiyama, Y.; Uebayasi, M.; Kitaura, K. *Chem. Phys. Lett.* **2002**, *351*, 475.
(62) Ishima, R.; Torchia, D. A.; Lynch, S. M.; Gronenborn, A. M.; Louis, J. M. *J. Biol. Chem.* **2003**, *278*, 43311.

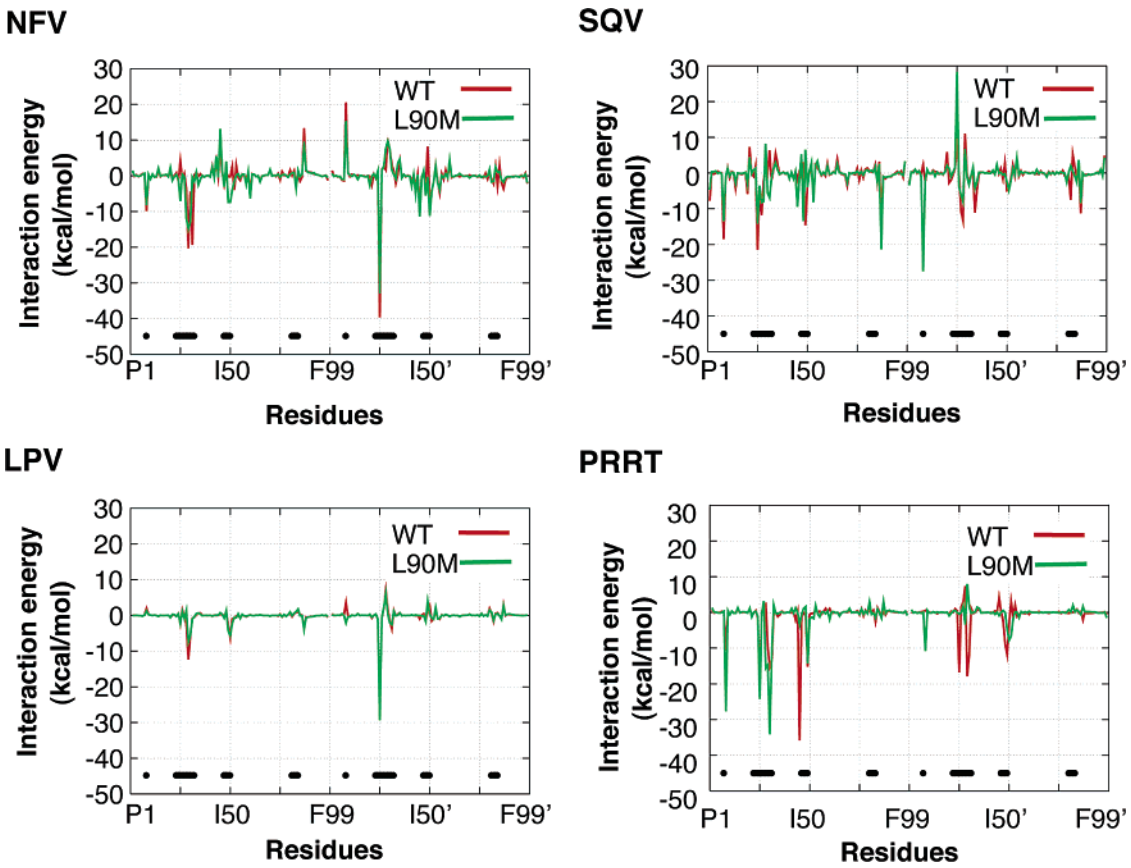

Figure 5. Interresidue interaction energies between PR and ligand calculated by FMO−HF/6-31G. Black lines below indicate the location of the active site residues (R8, L23-V32, I47-I50, P81-I84, R8′, L23′-V32′, I47′-I50′, P81′-I84′).

comparison of ΔG, the calculated inhibitory order for NFV, SQV, and LPV is not compatible with that determined by experiments[63] (Supporting Information Table S4). In contrast, when compared with experimental ΔH, the order in calculated ΔG for the inhibitors is consistent with the experimental measurements. That is because our MM/PBSA calculations do not include entropic terms. Hence, the incorporation of an entropic term will enable us to accurately predict the potency of a new drug by MD simulations.

LPV is one of the most promising drugs for AIDS treatment as shown in the present study. However, as the number of mutations increases, the efficacy of LPV decreases. For example, according to Virologic phenotypic assays, patient-derived HIV-1 confers 20-fold resistance against LPV. The PR sequence of this HIV-1 includes some drug resistant-related mutations (L10I, K20R, M36I, R41K, M46I, F53L, Q61N, L63P, A71V, T74S, V82T, N88S, L90M, I93L). Results of our additional simulation of this resistant PR with LPV have indicated a decrease in inhibitory efficacy ($\Delta G_b = -59.5$ kcal/mol, $\Delta\Delta G_b = +2.3$ kcal/mol) (Supporting Information Figure S4). These mutations decrease the number of hydrogen bonds between LPV and this clinically derived PR (Supporting Information Table S5). Furthermore, the mutations change the conformations at the flap and 80's loop regions (Supporting Information Figure S5). A design to remove the collisions at these regions will further enhance the efficacy of LPV. It should be emphasized that most of the mutated residues are located at the nonactive site of PR. Thus, to create more potent drugs, it is important to clarify the roles of the drug-resistant related nonactive site residues.

On the basis of the findings obtained in this study, we suggest the following strategy for the design of HIV-1 PR inhibitors. First, inhibitors should not contain a large ring such as a dodecahydroisoquinoline ring at P1/P1′ subsites; a linear chemical group is favorable. Second, to remove the collisions at the 80's loop and the flap region, functional groups at P2P1/P1′P2′ subsites of inhibitors should be in the same size as those of PRRT. Third, inhibitors should interact only with limited PR residues such as D25/D25′ and D29/D29′. Finally, inhibitors should not make unnecessary contact with any residues even in WT PR.

In summary, the mechanism of resistance due to the nonactive site mutation L90M has been clarified through theoretical calculations. The 90th residue of HIV-1 PR is located at the dimer interface and has no direct contact with ligand chemicals. The simulations demonstrate that the nonactive site mutation affects conformation of the binding cavity and ligand-binding affinity at the active site. The results of the present study have revealed the drug resistance mechanism of nonactive site mutation and provide a clue for designing a promising drug to reduce the drug resistance due to nonactive site mutation. Adaptive drugs,[64−67] which have the ability to inhibit several variants of a targeting enzyme, are needed in anti-HIV therapy.

(63) Yanchunas, J., Jr.; Langley, D. R.; Tao, L.; Rose, R. E.; Friborg, J.; Colonno, R. J.; Doyle, M. L. *Antimicrob. Agents Chemother.* **2005**, *49*, 3825.
(64) Velazquez-Compoy, A.; Freire, E. *J. Cell. Biochem.* **2001**, *S37*, 82.
(65) Freire, E. *Nat. Biotechnol.* **2002**, *20*, 25.
(66) Ohtaka, H.; Schon, A.; Freire, E. *Biochemistry* **2003**, *42*, 13659.
(67) Ohtaka, H.; Freire, E. *Prog. Biophys. Mol. Biol.* **2005**, *88*, 193.

Some reviews have suggested strategies for the design of adaptive inhibitors for HIV-1 PR.[64,66−69] These strategies, however, do not give sufficient consideration to the structural effects due to nonactive site mutations. The findings of this work should be useful for producing practical adaptive drugs.

Acknowledgment. This work was supported by a Health and Labor Science Research Grant for Research on HIV/AIDS from the Ministry of Health and Labor of Japan and by JSPS Research Fellowships for Young Scientists and a grant-in-aid for JSPS Fellows. A part of this work was also supported by a grant from the Japan Science and Technology Agency.

(68) King, N. M.; Prabu-Jeyabalan, M.; Nalivaika, E. A.; Schiffer, C. A. *Chem. Biol.* **2004**, *11*, 1333.
(69) Prabu-Jeyabalan, M.; Nalivaika, E. A.; Schiffer, C. A. *Structure* **2002**, *10*, 369.

Supporting Information Available: RMSD plots during MD simulations, determination of protonation states of catalytic aspartates in the SQV and/or LPV complex models, a list of hydrogen bond networks in each model, RMSF plot of main chain atoms N, Cα and C in each model, a list of differences between RMSD values (Å) of the main chain atoms in WT and L90M models, comparison of the computed L90M model and the crystal structure (1FG7), comparison of computed ΔG with experimental ΔG and ΔH, results of analyses of the MD simulations of clinically derived HIV-1 PR in complex with LPV, and a complete list of author citations with more than 10 authors. This material is available free of charge via the Internet at http://pubs.acs.org.

JA060682B